Original Article

Prognostic significance of pyroptosis-related factors in lung adenocarcinoma

Ximing Lin[1]^, Tian Zhou[2], Shaopu Hu[1], Lihui Yang[1], Zepei Yang[1], Haoyue Pang[1], Xiangnan Zhou[1], Ruikang Zhong[1], Xueni Fang[1], Zhongyang Yu[1], Kaiwen Hu[2]

[1]Graduate School, Beijing University of Chinese Medicine, Beijing, China; [2]Department of Oncology, Dongfang Hospital, Beijing University of Chinese Medicine, Beijing, China

Contributions: (I) Conception and design: K Hu, X Lin, T Zhou; (II) Administrative support: K Hu; (III) Provision of study materials or patients: S Hu, Z Yang, H Pang; (IV) Collection and assembly of data: X Lin, L Yang, X Zhou, Z Yu; (V) Data analysis and interpretation: X Lin, R Zhong, X Fang; (VI) Manuscript writing: All authors; (VII) Final approval of manuscript: All authors.

Correspondence to: Kaiwen Hu. Department of Oncology, Dongfang Hospital, Beijing University of Chinese Medicine, No. 6 Fangxingyuan 1st Block, Fengtai District, Beijing 100078, China. Email: kaiwenh@163.com.

Background: Numerous studies have revealed that the abnormal expression of pyroptosis-related genes is closely related to the prognosis of lung adenocarcinoma (LUAD); however, a comprehensive analysis has yet to be conducted. This study aimed to reveal the influence of pyroptosis-related genes on the prognosis of LUAD and establish a prognostic model based on those genes, in order to evaluate the prognosis of LUAD.

Methods: The data of tumor and normal samples were downloaded from The Cancer Genome Atlas (TCGA) and Gene Expression Omnibus (GEO) databases. Differential analysis was used to identify pyroptosis-related genes (obtained from the GeneCards database) that were differentially expressed (DE) in TCGA database. Univariate and stepwise multivariate Cox proportional hazards regression analyses were used to screen feature genes related to LUAD overall survival (OS) and construct gene signature. Gene set enrichment analysis (GSEA) was then performed to reveal potential functions related to gene signature. Finally, the Cell-type Identification by Estimating Relative Subsets of RNA Transcripts (CIBERSORT) algorithm was used to reveal distinctions in each cell-subtype groups in the immune landscape of LUAD.

Results: Overall, 26 DE genes (DEGs) associated with pyroptosis were obtained. Among them, 4 (*MKI67*, *BTK*, *MST1*, and *TUBB6*) were selected as prognostic genes and a 4-gene signature with a good prognostic performance in the TCGA and GEO was constructed. The gene signature was shown to be an independent prognostic factor of LUAD in subsequent analysis. Functional enrichment indicated that the 4-gene signature may participate in the tumorigenesis and development of LUAD through various pathways related to tumor progression to play a prognostic role in LUAD. Additionally, the results of the immune landscape indicated that the 4-gene signature may affect the prognosis of LUAD via cooperating with changes in the immune microenvironment.

Conclusions: The key biomarkers and pathways identified in this study would deepen the comprehension of the molecular mechanism of pyroptosis in LUAD. More importantly, the 4-gene signature may serve as a novel potential prognostic model for LUAD.

Keywords: Pyroptosis-related genes; prognosis; lung adenocarcinoma (LUAD); gene signature; immune landscape

Submitted Dec 29, 2021. Accepted for publication Mar 04, 2022.
doi: 10.21037/jtd-22-86
View this article at: https://dx.doi.org/10.21037/jtd-22-86

^ ORCID: 0000-0002-8406-1817.

Introduction

Lung cancer (LC) is one of the most common neoplasia and the leading cause of worldwide cancer-related lethality (1). Lung adenocarcinoma (LUAD) comprises the largest proportion in LC, accounting for 40% of all cases, with a survival rate of only 4–17% (2). Canonical first-line treatments for LUAD including surgery, chemotherapy, and radiotherapy along with recent popular target agents and immunotherapy (3). Nevertheless, despite the use of multiple therapeutic modalities for the past several decades, the improvement in survival duration for LUAD has remained unfavorable (4). It is necessary to identify a new series of biomarkers that could help to foresee the LUAD prognosis, especially in the level of multi-gene signatures. Pyroptosis has become one of the frontier hotspots of tumor therapy over recent years (5). Research has demonstrated that high expression of gasdermin D (GSDMD), a crucial pyroptotic effector, independently indicates a poor outcome in LUAD (6). Based on the former discovery, we postulated that a set of pyroptotic gene signatures might deliver deeper insight into the prognostic value of LUAD.

Pyroptosis is an inflammatory mode of regulated cell death (RCD) (7-9). It presents pore-forming morphological characteristics such as cell swelling, plasma membrane lysis, chromatin condensation, DNA fragmentation, and intact nucleus, with subsequent release of damage-associated molecular patterns (DAMPs) and pro-inflammatory factors such as interleukin (IL)-1β/18 (10). Although apoptosis and pyroptosis are both processes of RCD, apoptosis is a non-inflammatory mode with intact and packed morphological features (11). The gasdermin family is the essential member of the pyroptotic pathway, where activated gasdermin-combined lipid membrane oligomers slot pore channels and trigger pyroptosis. It has been shown that GSDMD is cleaved by caspase-1/4/5/11 and exposes pore-forming gasdermin N-terminal domain (GSDM-NT) in the inflammasome pathway (12-14). Certain stimulative signals induce non-inflammatory pyroptosis by cleavage of GSDME via activated caspase-3 (15,16). Pyroptosis plays a bidirectional reaction in tumorigenesis interestingly. While some research discovered the anti-tumor effect of pyroptotic mechanism in other tumors, a few researches announced the promotive action of pyroptosis in the development of LUAD. For example, GSDMD, one of crucial members of pyroptosis, was clarified to promote the development of LUAD via phosphoinositide 3-kinase (PI3K)/Akt/mammalian target of rapamycin (mTOR) pathway (6). However, a single biomarker of gasdermins cannot reveal the effective prediction, exposing that to discover a pyroptosis-related gene signature label is needed instead. Some previous studies have reported pyroptosis-related hub genes and raised their prognostic models (17-19). Here, we observed a wider range of pyroptosis-related genes that could be included in the screening scope and utilized the methods with correlation to prognostic detectable.

Pyroptosis acts as a bridge between tumor-infiltrating immune cell (TIIC) and tumor tissues. Specifically, the discharge of pyroptosis-derived cytokines, especially IL-1β and IL-18, not only alters the TIIC microenvironment and promote the tumorigenesis by escaping immune surveillance, but also can also triggers TIIC recruitment and help immune therapies (20). From this point, we also made an exploratory of TIIC estimation based on pyroptosis-related gene signature in this study.

In this study, we investigated the key biomarkers and pathways that may provide a deeper perspective on the molecular mechanism of LUAD. We also observed pyroptosis-related genes contributing to prognosis in LUAD, and a clinical model of multi-candidate biomarkers was established for anticipating dependable prognosis for LUAD. We present the following article in accordance with the TRIPOD reporting checklist (available at https://jtd.amegroups.com/article/view/10.21037/jtd-22-86/rc).

Methods

Data source

We obtained gene expression data and corresponding clinical information of 519 cases of LUAD and 58 cases of normal samples from The Cancer Genome Atlas (TCGA; https://www.cancer.gov/about-nci/organization/ccg/research/structural-genomics/tcga) database to use as a training set. Among them, 490 LUAD samples with complete survival information were involved in the subsequent survival analysis. The GSE31210 dataset (226 LUAD samples in total; https://www.ncbi.nlm.nih.gov/geo/query/acc.cgi?acc=GSE31210) obtained from the Gene Expression Omnibus (GEO) database was used as an external verification set to test the validity of gene tags. The GeneCards database (https://www.genecards.org/) was used to find 110 pyroptosis-related genes (Table S1). The study was conducted in accordance with the Declaration of Helsinki (as revised in 2013).

Differential expression analysis

First, we extracted 110 pyroptosis-related gene expression matrices from TCGA expression profile data. Next, the DESeq2 package in R (https://www.r-project.org/) was used for screening the pyroptosis-related differentially expressed genes (DEGs) between the LUAD and normal groups. We set $|\log_2$ fold change (FC)$|$ >1 and false discovery rate (FDR) <0.05 as the cut-off criteria to indicate significant statistical difference. In this study, 98 of 110 pyroptosis-related genes were expressed in TCGA-LUAD. The ggplot2 and pheatmap packages in R were used to plot volcano maps and cluster heatmaps.

Prognostic signature construction and validation

To investigate the potential role of pyroptosis-related DEGs in LUAD survival, each pyroptosis-related DEG was assessed by univariate Cox regression analysis and stepwise multivariate Cox proportional hazards regression model in the TCGA-LUAD cohort. Finally, genes with P<0.05 were utilized to construct a prognostic signature and calculate the risk score of each sample. The polygenic risk score was calculated by using following formula: risk score = expression of $Gene_1 \times \beta_1 Gene_1$ + expression of $Gene_2 \times \beta_2 Gene_2$ + … + expression of $Gene_n \times \beta_n Gene_n$. Here, the step multivariate Cox proportional hazards regression model was used to generate β, which represented the regression coefficient. The accuracy of the prognostic signature was evaluated by employing the time-dependent receiver operating characteristic (tdROC) curve, which was implemented in the SurvivorROC package. To verify this prognostic signature, LUAD patients from the GSE31210 dataset were treated as an independent external verification cohort.

Independent prognostic analysis

To assess values of independent prediction for four-gene signature in LUAD, univariate and multivariate Cox regression analyses were performed. In this study, age, gender, tumor stage, and pathological tumor, node, metastasis (TNM) stage were included in this analysis, which were obtained from the TCGA-LUAD cohort.

Gene set enrichment analysis (GSEA)

To explore potential mechanisms underlying correlation between prognostic signature and LUAD, GSEA was conducted between high- and low-risk groups in the TCGA cohort through clusterProfiler package in R. The c5 reference gene set and c2 reference gene set from Molecular Signatures Database (MSigDB; https://www.gsea-msigdb.org/gsea/msigdb/) were used as the Gene Ontology (GO) gene set and Kyoto Encyclopedia of Genes and Genomes (KEGG) gene set, respectively. By running GSEA, normalized enrichment scores and P values were created. A P value <0.05 was considered statistically significant. In GO analysis, we only focused on the consequences of the biological process (BP) category. The detailed results of the cellular component (CC) and molecular function (MF) were also derived (tables available at https://cdn.amegroups.cn/static/public/jtd-22-86-1.xlsx; https://cdn.amegroups.cn/static/public/jtd-22-86-2.xlsx).

Evaluation of immune cell type components

To evaluate the various abundance of 22 TIIC types between low- and high-risk of LUAD cases, the Cell-type Identification by Estimating Relative Subsets of RNA Transcripts (CIBERSORT) analytical tool with the LM22 signature matrix was performed. We then measured the P value for the deconvolution of each specimen through Monte Carlo sampling. Cases were enrolled with CIBERSORT P<0.05, the value of which controlled taking in and out (table available at https://cdn.amegroups.cn/static/public/jtd-22-86-3.xlsx). All values of the estimated 22 TIIC proportions always summed up to 1 for every sample.

Statistical analysis

The independent sample *t*-test was utilized to compare the test of expression between both groups. The DEG screening was adjusted by FDR through the Benjamini-Hochberg methods. Survival analysis performed with the Kaplan-Meier (K-M) method was checked by the log-rank test. A P value <0.05 was considered to achieve statistical significance. Statistical analyses were conducted using the R software.

Results

Identification of DE-pyroptosis-related genes in LUAD

Following TCGA-LUAD database analysis in the DESeq2 package, 26 LUAD-associated DE-pyroptosis-related

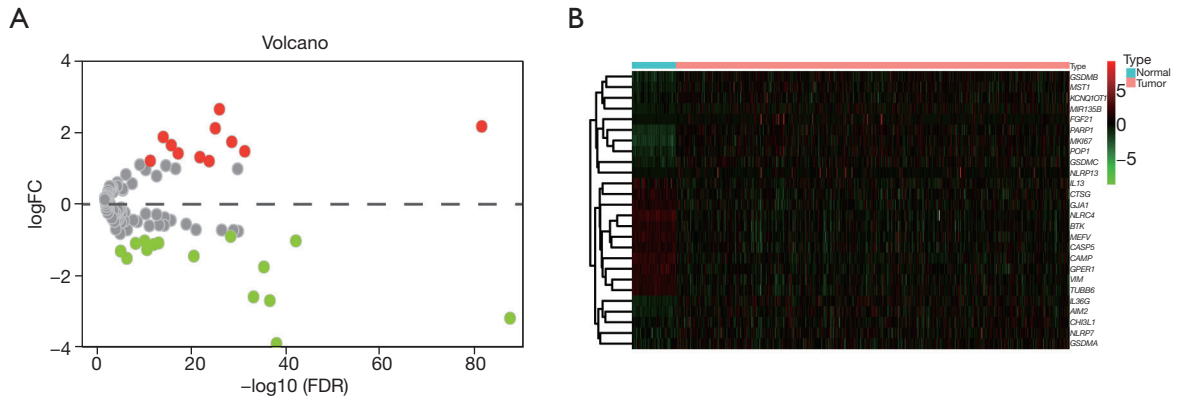

Figure 1 DEGs expression profile in the TCGA-LUAD dataset. (A) The volcano plot of DEGs in the TCGA-LUAD dataset. Red dots on the upper area represent upregulation of DEGs, whereas green dots on the bottom represent downregulation of DEGs. The gray represents no statistically significant difference in gene expression. (B) Heatmap of DEGs between the LUAD samples and the normal samples. FC, fold change; FDR, false discovery rate; DEGs, differentially expressed genes; TCGA-LUAD, The Cancer Genome Atlas-lung adenocarcinoma.

genes were successfully identified. Notably, 15 pyroptosis-related genes were markedly downregulated, while 11 genes were upregulated in LUAD tissues contrasted to normal counterparts (*Figure 1A*; Table S2). The hierarchical clustering heatmap of the above 26 genes is shown in *Figure 1B*, where the red and green dots represent the up and downregulated genes, respectively. The 26 genes obtained from the differential analysis were included as candidate genes for further analysis.

Screening of feature genes for the prognosis of LUAD

Univariate Cox regression analysis was performed to determine the prognostic value of candidate genes. It was revealed that 10 of 26 candidate genes were significantly associated with OS in LUAD. The *MKI67*, *PARP1*, *POP1*, *TUBB6*, and *GJA1* genes were considered as risk factors [hazard ratio (HR) >1], while the remaining 5 prognostic candidate genes (*NLRC4*, *BTK*, *CAMP*, *MST1*, and *CTSG*) were identified as protective factors (HR <1; *Figure 2A*). Stepwise multivariate Cox regression analysis was applied to define the stable markers, which would build a clinical survival prognostic model, from 10 OS-related candidate genes. The 4 parameters for building the prognostic model are presented in *Figure 2B*, and 2 filter markers (*MKI67* and *TUBB6*) were shown to be associated with increased risk (HR >1; Table S3). Subsequently, K-M curve analysis was employed for each gene, with the median value of expression as the cut-off (*Figure 2C*). Here, the expression of *MST1* was not significantly associated with OS (P=0.24), and the significance of which was not obvious in formal analysis (P=0.055). After comprehensive consideration, we continued to use it as a key prognostic gene to construct a prognostic model with *MKI67*, *BTK1*, and *TUBB6*. Ultimately, a risk score formula indicating survival prediction for each sample was developed based on the 4 key genes, along with their coefficients and expression levels, which was presented as follows: (0.13 × expression level of *MKI67*) + (−0.27 × expression level of *BTK*) + (0.23 × expression level of *TUBB6*) + (−0.14 × expression level of *MST1*).

Evaluation and verification of the value of the prognostic signature

To validate the robustness of the 4 pyroptosis-related genes, the capability of the prognostic model to stratify the high- or low-risk group in the TCGA-LUAD dataset was evaluated. A total of 490 patients with LUAD were bisected into a high- or low-risk group with the standard of the median value of the risk score. It showed that the high-risk group by this scoring system was greatly distinguishable from the low-risk group and was linked with the poorer prognosis from the K-M curve analysis (*Figure 3A*). The 1-, 3-, and 5-year area under the curve (AUC) of the tdROC was 0.672, 0.689, and 0.631, respectively (*Figure 3B*), corroborating the tolerable prediction efficiency of the 4-gene signature in OS. Consecutively, as exhibited in the heatmap, the expression of *MST1* and *BTK* increased in the low-risk group, while *MKI67* and *TUBB6* were

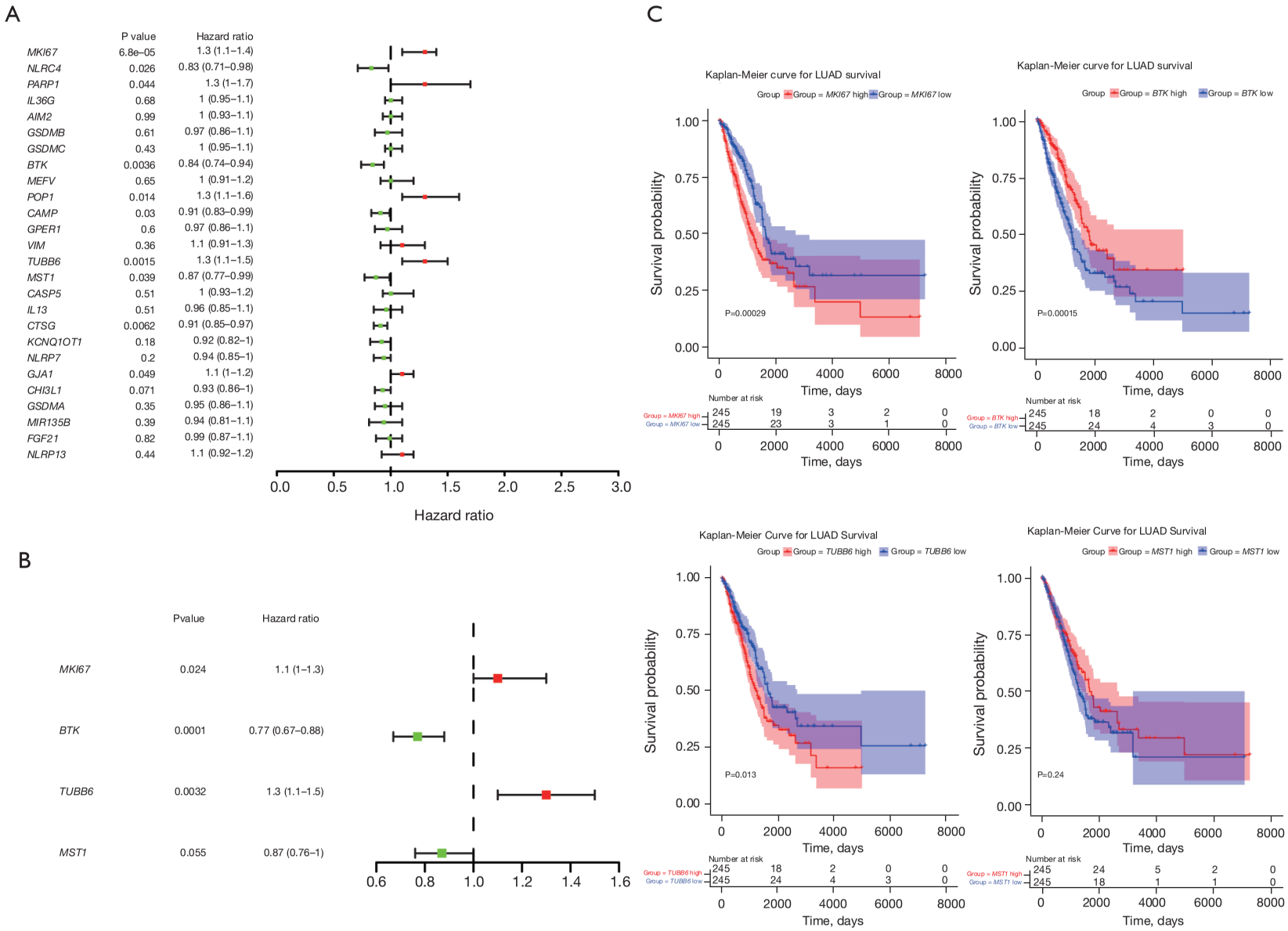

Figure 2 The univariate and multivariate Cox regression analysis for prognostic features screening. (A) Univariate Cox regression analysis to predict prognostic factors associated with patient survival. (B) Multivariate Cox regression analysis of 4 prognostic genes. (C) Kaplan-Meier OS curves according to the expression levels of *MKI67*, *BTK*, *TUBB6*, and *MST1*. LUAD, lung adenocarcinoma; OS, overall survival.

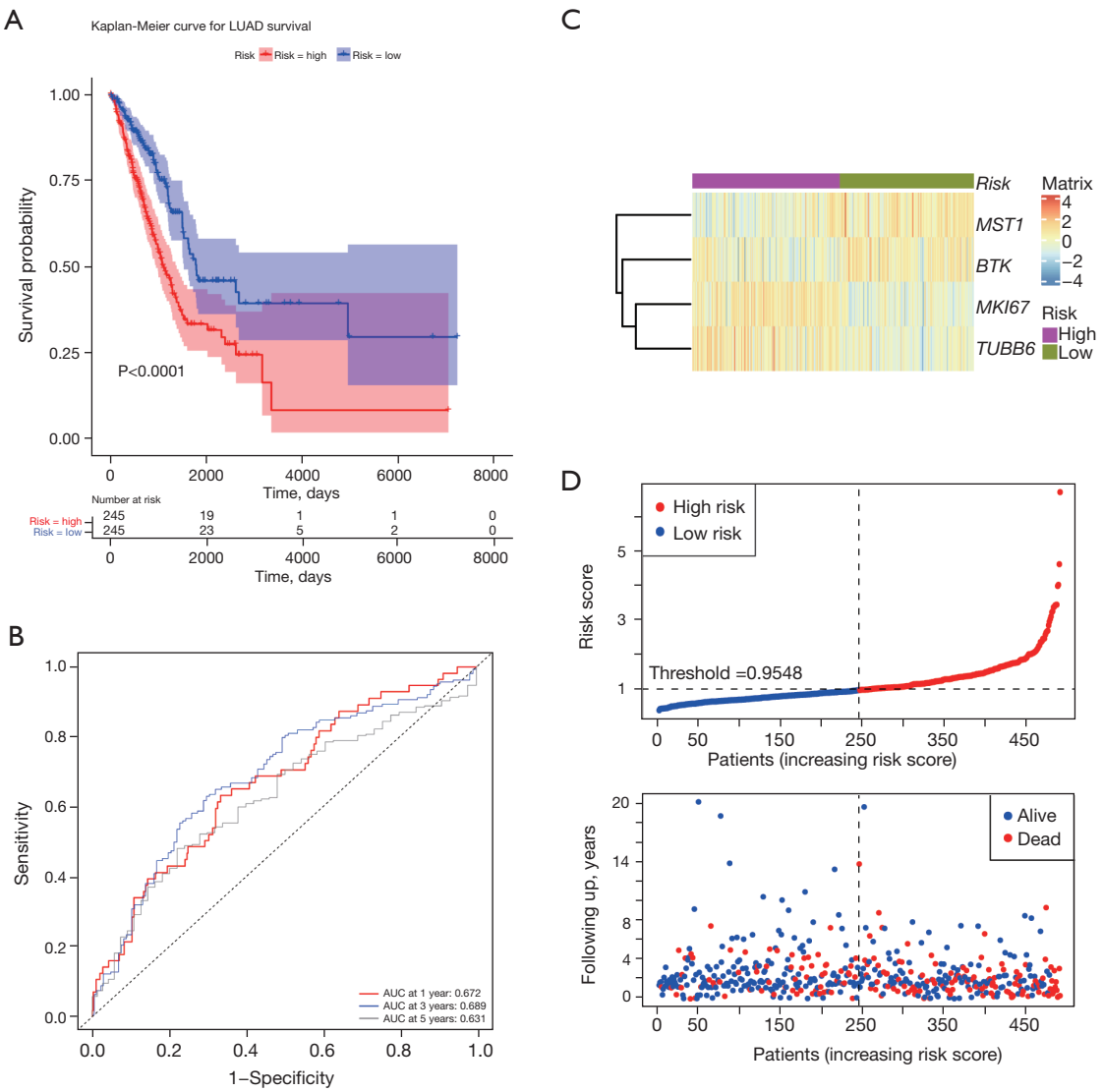

Figure 3 The gene signature-based risk score built in the TCGA-LUAD dataset. (A) The Kaplan-Meier survival curves of the 4-gene signature in the training set. All samples were separated into high- and low-risk groups depending on the median value for the risk scores. (B) ROC curve evaluating effectiveness of risk model in the training set. (C) Heatmap of the expression profiles of the four prognostic genes in low- and high-risk groups. (D) Risk curve and the distributions of the 4-gene signature and survival status of patients in the training set. LUAD, lung adenocarcinoma; AUC, area under the curve; TCGA-LUAD, The Cancer Genome Atlas-lung adenocarcinoma; ROC, receiver operating characteristic.

overexpressed in the high-risk group (*Figure 3C*). In succession, it was indicated that patients with a risk score of 0.9548 or higher generally survived worse than the other group of patients viewing from the distribution of risk scores and survival status (*Figure 3D*).

Furthermore, verification of the prognostic capacity of the promising marker in the GSE31210 dataset followed. Survival information and corresponding gene expression data of 226 LUAD patients from the validation set were gathered and imported into the same formula to calculate the risk score of each patient. Using the median risk score as a cut-off value (0.5613), the LUAD samples in the validation set were divided into high- (n=113) and low-risk (n=113) groups, and the survival status and 4-gene expression manners of the 2 groups were compared (*Figure 4A,4B*). A similar conclusion made by the training set was confirmed: the high-risk group had poorer OS. As shown in *Figure 4C*, a good sensitivity of the risk score

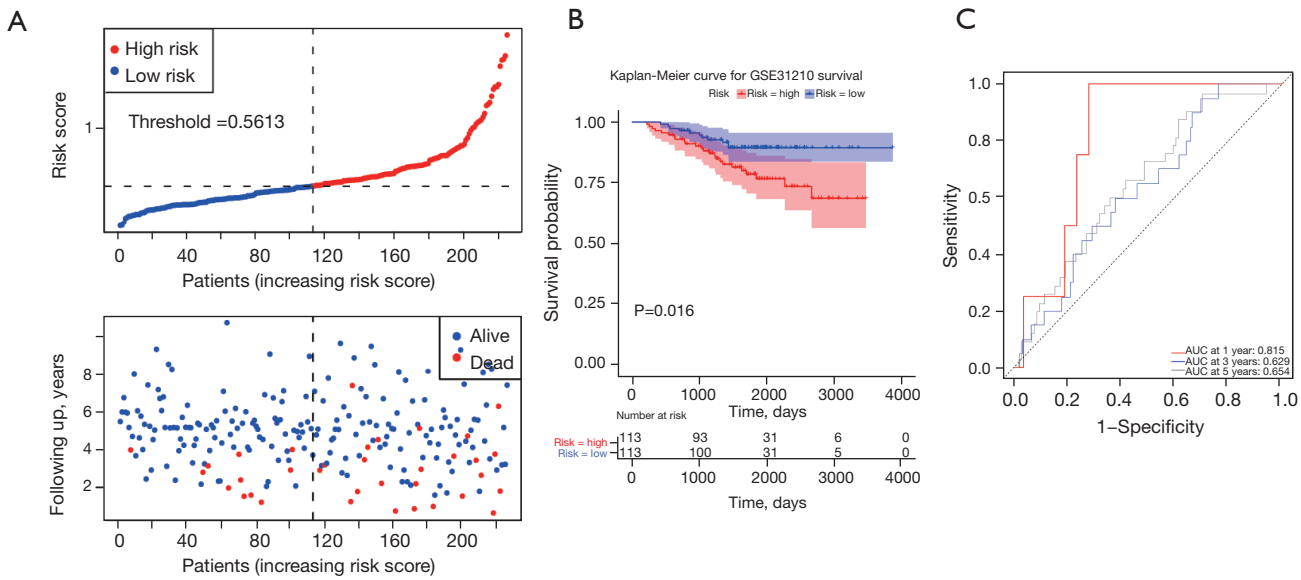

Figure 4 The predictive function of gene signature-based risk score verified in the GSE31210 dataset. (A) Risk curve and the distributions of survival status in 2 groups in the validation set. (B) The Kaplan-Meier survival analysis in the validation set. All samples were separated into 2 groups depending on the threshold of the risk scores. (C) ROC curve evaluating effectiveness of risk model in the validation set. AUC, area under the curve; ROC, receiver operating characteristic.

algorithm was certified with the AUCs of the 4-gene signature corresponding to 1, 3, and 5 years of OS were 0.815, 0.629, and 0.654, respectively.

Risk score and pathologic T and N stage as independent prognostic factors for LUAD

Given the independent prognostic value of the 4 pyroptosis-related gene signature, the risk score itself was identified through the univariate and multivariate Cox regression analysis. The TCGA-LUAD dataset suggested that the risk score, pathological TNM stage, and tumor stage were prognostic elements associated with OS (all P<0.05), while age and gender were not associated with the outcome indicator, as evidenced by the forest map of the univariate Cox regression (*Figure 5A*; Table S4). In sequence, the risk score, pathologic T stage, and pathologic N stage were the chosen potential factors in multivariable Cox regression analyses (*Figure 5B*; Table S5). The heatmap showed the expression levels of the 4-gene signature and the distribution of clinicopathological features between low- and high-risk TCGA-LUAD patients (*Figure 5C*). These statistical operations ascertained that the risk score based on the 4-gene signature could be an independent predictive factor for LUAD patients.

Enriching multiple tumor-associated pathways of the risk group system

In consideration of the risk score derived from the 4-gene signature in connection with some important signaling pathways, GSEA analysis was applied to uncover the relating pathways. The GSEA-GO enrichment results demonstrated that immune response, cell cycle, vasculature development, response to oxidative stress, DNA repair, and so on, were significantly enriched (*Figure 6A-6E*; table available at https://cdn.amegroups.cn/static/public/jtd-22-86-4.xlsx). Consistent with the GO analysis, the GSEA-KEGG results suggested that genes were involved in the DNA replication, mismatch repair, and cell cycle pathways (*Figure 6F-6J*). Besides, the risk group system was accompanied by the p53 signaling pathway, cAMP signaling pathway, ether lipid metabolism, peroxisome proliferator-activated receptor (PPAR) signaling pathway, fatty acid degradation, porphyrin and chlorophyll metabolism, and so on (table available at https://cdn.amegroups.cn/static/public/jtd-22-86-5.xlsx). These pathways were significantly correlated with tumor progression.

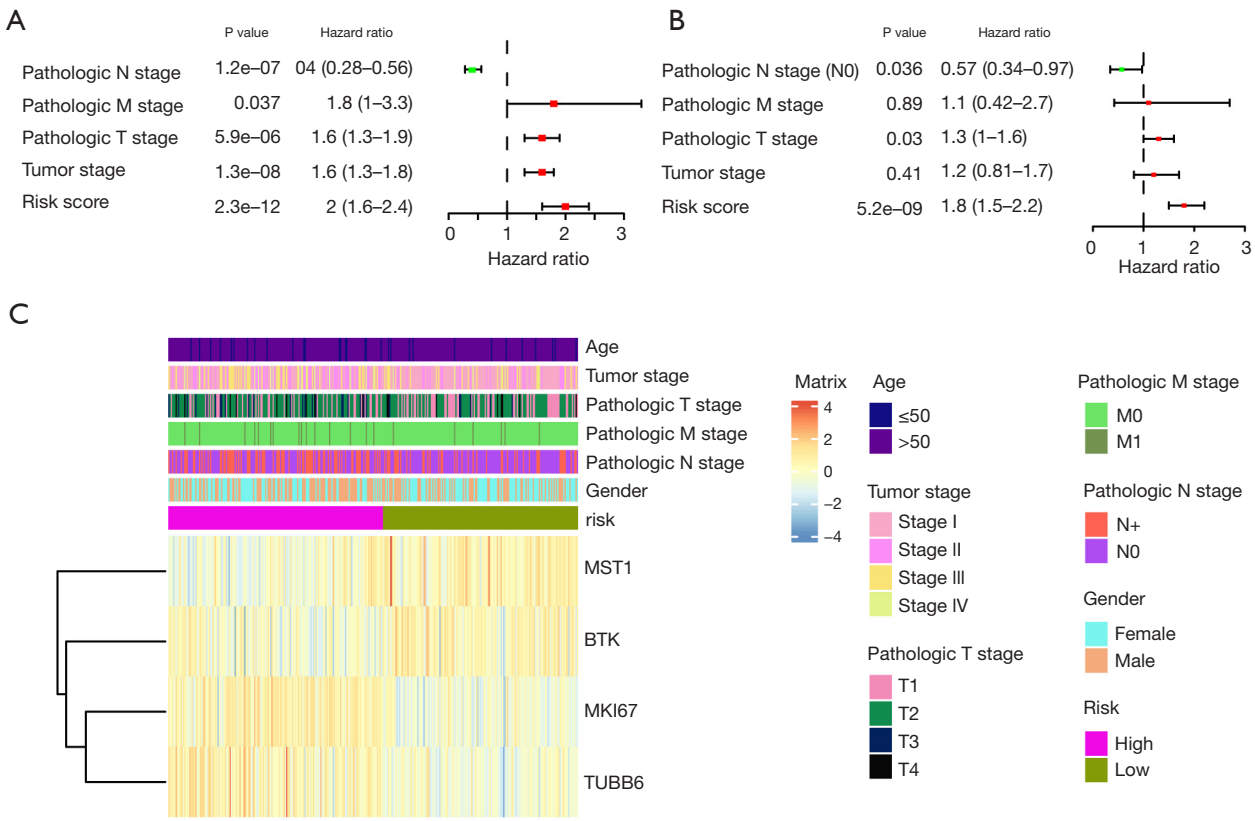

Figure 5 Identifying the independent prognostic foothold of the gene-based prognostic model. Forest plot of univariate (A) and multivariate (B) analyses of OS based on the 4-gene signature and clinical variates in the TCGA-LUAD dataset. (C) Summarized heatmap of the distribution of clinical characteristics and the 4-gene signature in TCGA. OS, overall survival; TCGA-LUAD, The Cancer Genome Atlas-lung adenocarcinoma.

Immune landscapes between LUAD patients with low- and high-risk scores

The exploratory finding was conducted through CIBERSORT, where the variance concerning the scales of 22 TIICs between low- and high-risk LUAD patients was assessed. The proportion of immune cells in each LUAD case was diverse, which indicated that the altered immune cells within the tumor may be an inherent feature representing individual variation (*Figure 7A*). The high-risk LUAD group contained expressively higher ratios of B cells memory, plasma cells, T cells CD4 memory activated, natural killer (NK) cells activated, macrophages M0, dendritic cells (DCs) activated, and neutrophils ($P<0.05$), while significantly lower proportions of B cells naive, T cells CD4 memory resting, monocytes, and DC resting than the low-risk LUAD group (*Figure 7B*). Consequently, the risk score system may cooperate with the heterogeneity of the immune tumor microenvironment (TME) in LUAD to have a critical impact on the identification of prognosis and had significant clinical implications.

Discussion

Present state of diagnosis and therapy in LUAD

Combined strategies of surgery, chemotherapy, radiotherapy, targeted agents, and recently immunotherapy are extensively performed in LUAD (3). Unsatisfactorily, the effectiveness of therapy is less remarkable in advanced LUAD due to the acquired resistance (21,22). In another aspect, LUAD performs more distinctive genomic alterations than other LC types and is accessible to present molecular heterogeneity by genome sequencing technology (23,24). Therefore, genetic mutation-based analysis is supposed to facilitate the therapeutic decisions in improving prognosis.

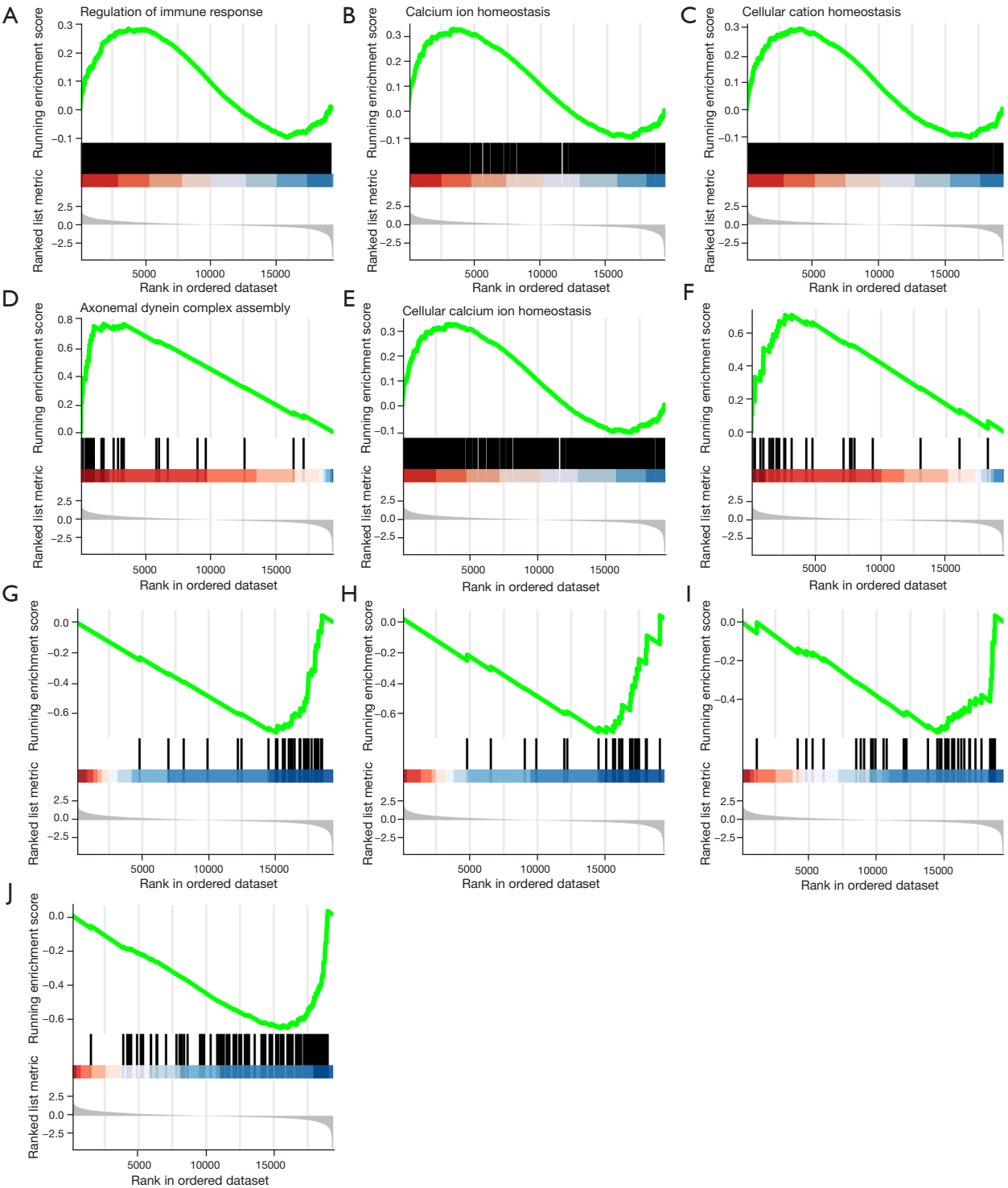

Figure 6 GSEA enrichment results of first few in BPs of GO and KEGG. (A-E) GSEA enrichment in BPs of GO such as regulation of immune response, calcium ion homeostasis, cellular cation homeostasis, axonemal dynein complex assembly, and cellular calcium ion homeostasis. (F-J) GSEA enrichment in KEGG such as linoleic acid metabolism, DNA replication, mismatch repair, homologous recombination, and cell cycle. GSEA, gene set enrichment analysis; BP, biological process; GO, Gene Ontology; KEGG, Kyoto Encyclopedia of Genes and Genomes.

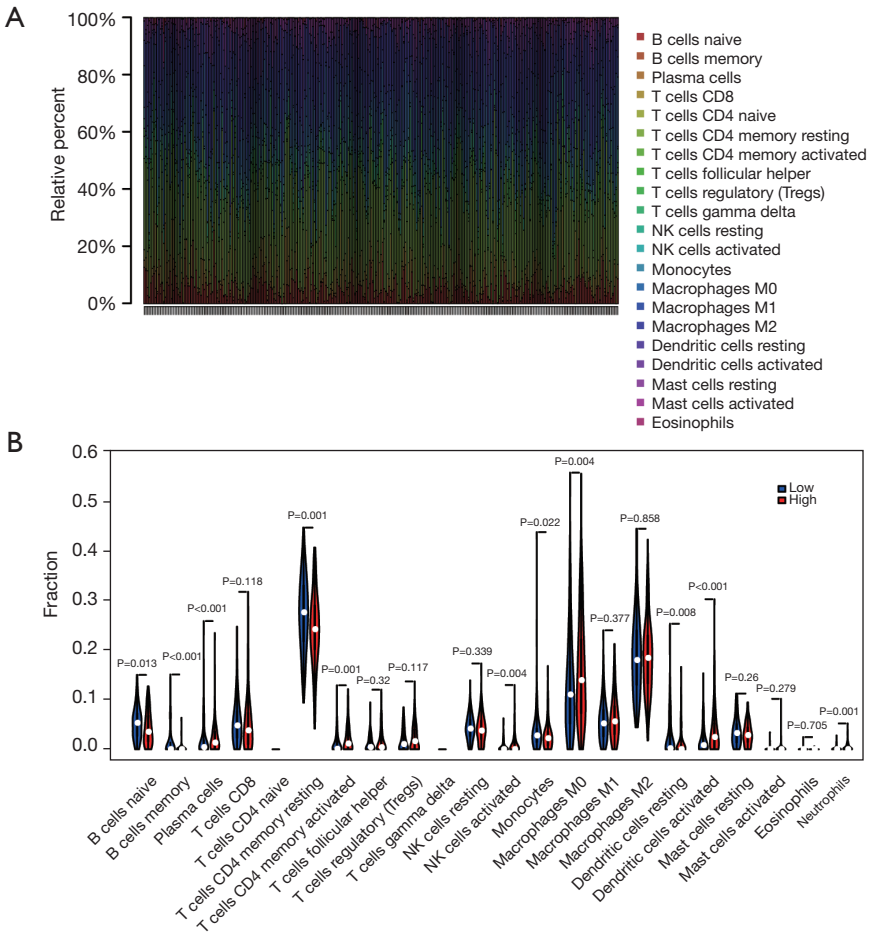

Figure 7 The landscape of immune infiltration between low- and high-risk groups. (A) The relative percentage of 22 TIICs in 302 samples from the TCGA-LUAD dataset. (B) The discrepancy of immune infiltration between low- and high-risk groups (P<0.05 was considered statistically significant). NK, natural killer; TIIC, tumor-infiltrating immune cell; TCGA-LUAD, The Cancer Genome Atlas-lung adenocarcinoma.

Connection of pyroptosis, pyroptosis-related hub genes, and immune microenvironment to LUAD

Pyroptosis is a pro-inflammatory manifestation of programmed cell death, traditionally seen as a protective mechanism by self-adjustment or treatments. In this study, we mainly focused on the enriched BP of the 4-gene signature tributed to LUAD, such as immune response, cell cycle, vasculature development, oxidative stress, and DNA repair.

Canonical pyroptosis induces downstream innate and adaptive immune reactions which progressively enhance anti-tumor effect via releasing intracellular molecules (25). Compound L61H10 simultaneously induces G2/M cell cycle arrest and transformation from apoptosis to pyroptosis (26). The protein GSDMD obstructs gastric cancer proliferation by inhibition of CyclinA2 and CDK2 with contributing to S to G2/M phase arrest (27). Piperlongumine analogue L50377 promotes pyroptosis via inducing reactive oxygen species (ROS) generation, which regulates the angiogenesis process (28,29). The *ZDHHC1* gene contributes to the increment of oxidative stress to promote pyroptosis for anticancer purposes (30). Additionally, *PLK1* inhibitor sensitizes cisplatin-treated DNA damage by negative regulation to DNA repair pathway and induces GSDME-mediated pyroptosis (31).

The pyroptosis-related 4-gene candidates (*MKI67*, *BTK*, *TUBB6*, and *MST1*) were combined to indicate the prognosis of LUAD in the present filter of the pre-clinical method. The *MKI67* gene (marker of proliferation *Ki-67*) encodes

a nuclear DNA-binding protein, *Ki-67*, which acts as a mitotic chromosome stabilizer by linking to and covering its surface (32). Thus, it has been widely used as a technological marker for cell proliferation in many diseases (33). *Ki-67* becomes the same role in the tumorigenesis of LUAD and its overexpression indicates declining OS in LUAD (34). It has been revealed as a poor indication in LUAD, and one of the influential factors in differentiation between LUAD subtypes (35). Simvastatin has been reported to inhibit the effect of *Ki-67* on tumor proliferation and migration via the pyroptosis pathway in A549 and H1299 cells (36). The results of our study were aligned with these findings. The *BTK* gene (Bruton tyrosine kinase) was originally known as an essential target for B cell development and in the treatment of B cell malignancies (37). The function of *BTK* in LUAD remains unknown yet. Unlike *BTK* has a lower expression in LUAD than normal tissues (38). Recently, *BTK* has been considered an oncogenic target in solid tumors (39). Anti-*BTK* targeted drug, Ibrutinib, fails to achieve ideally protective efficacy in LUAD, whereas Auranofin enhances Ibrutinib's activity in *EGFR*-mutant LUAD (40,41). Overexpression of p65-*BTK* groups, T790M-mutant, or erlotinib-resistant groups has been verified to selectively gain more benefits from *BTK* tyrosine kinase inhibitors (42,43). Meanwhile, a bioinformatical study reported that lower expression of *BTK* might be a protective predictor of LUAD (44). Controversially, *BTK* has been found as a tumor suppressor of p53-dependent senescence and apoptosis in other aspects (45,46). We found that *BTK* might play a role as a protective element related to pyroptosis in this prognostic study. The *TUBB6* gene (tubulin beta 6 class V) encodes one type of β-tubulin, a structural subunit of microtubular α/β-heterodimers, which contains several individual isotypes with regulatory expression and distribution characteristics varying in mitotic and tumoral tissues (47,48). *TUBB3*, paralog of *TUBB6*, is the main constituent of tubulin and microtubule, inferior and superior structures of cytoskeleton respectively (49). Microtubule signifies division and growth in LUAD, and this is identified as the target of microtubule stabilizer, as known as taxanes (50). Tubulin-binding agents (TBAs) have shown early anti-tumor effects, mainly via apoptosis (51). Simultaneously, TBAs have been approved for their great clinical value as a single agent or regime combination with chemotherapy in advanced non-small cell lung cancer (NSCLC) (52,53). The advent of resistance to TBAs comes to a new challenge (54). The expression of *TUBB3* has been reported as greatly increased in NSCLC and could be a prognostic and predictive factor of resistance to TBAs (55). Expression of *TUBB6* is largely decreased in most tumors, including LUAD; however, its direct mechanism has yet to be clarified (56). Our results highlight that *TUBB6* might provide another perspective towards prognostics in LUAD therapeutics. The *MST1/MSP* gene (macrophage stimulating 1/macrophage stimulating protein) is a secreted ligand mostly generated from the liver and activates its effect by binding to transmembrane tyrosine kinase receptor *RON* (recepteur d'origine nantais) mainly on the macrophage. The *MSP-RON* signaling pathway mediates inflammation and immune escape in physics (57). *RON* shares MET-like domain and function of ignition the tumorigenesis in LUAD (58). *MSP-RON* signaling pathway subsequently activates RAS-ERK and PI3K-Akt pathways to achieve development, migration, angiogenesis and chemoresistance in tumor cell (59). Whereas, the expression of *RON* in LUAD is not so highly distinct as breast, colon or pancreatic cancers, so another observation will be needed (60). Abrogation of *RON* expression resulted in a significant loss in viability and motility in NSCLC (61). Functional *MSP* inducing *RON* phosphorylation increases motility in H596, yet proliferation or apoptosis has not been observed (62). The *MST1* gene has been identified as a novel prognostic mitogen in lung squamous cell carcinoma (63). In our study, *MST1* was identified as a protective factor. Similarly, the same conclusions were drawn from the finding that the locating region of *MST1* and *RON* coding genes sparks tumor suppressor activity and undergoes the frequent loss of heterozygosity (61).

Regulation of immune response was cardinally clustered in the pyroptosis-related 4-gene signature of LUAD. In addition, a previous study indicated an oncogenic role for GSDMD, one of the cardinal components of pyroptosis, in LUAD. On this basis, we considered poor outcome of LUAD might be attributed to coaction of the fractions of TME, and the immune landscape was subsequently analyzed through CIBERSORT. Among 7 high proportions of immunocytes between the landscapes, several cell lines have been reported as associated with malignant prospects in LUAD. A high concentration of plasma cell infiltration was confirmed as relating to the least favorable prognosis in LUAD (64). Besides, *BTK* is down-regulated as a transition from mature B cells to plasma cells (65). Abundant NK cell activated density is correlated with poor prognosis, and *BTK* is required for NK cell development (66,67). Macrophage presence is correlated with poor prognosis, since tumor-associated macrophages generally fuel pro-tumorigenic

participation such as metastasis, angiogenesis, and immunosuppression (68,69). Additionally, high neutrophil proportion indicates a higher risk of LUAD (70).

The pyroptosis-related gene signature in this study holds some promising properties for in-depth research and long-term application in LUAD. The predictive pyroptosis-related gene signature would also be able to indicate prospective immune-related therapies in LUAD.

Conclusions

In conclusion, this study identified 26 DEGs with comprehensive bioinformatics analysis, provided their molecular mechanisms, and selected the potential biomarkers, *MKI67*, *BTK*, *MST1*, and *TUBB6*, which were grouped to predict progression of LUAD. However, further experiments *in vitro* and *in vivo* are required to validate the characteristics of these screened genes and pathways in pyroptosis progression in LUAD. In the future, we will continue to focus on pyroptosis function in LUAD through clinical and experimental studies.

Acknowledgments

We are grateful for the free access of TCGA and GEO databases.

Funding: This work was supported by the National Key R&D Program of China (2018YFC1705102).

Footnote

Reporting Checklist: The authors have completed the TRIPOD reporting checklist. Available at https://jtd.amegroups.com/article/view/10.21037/jtd-22-86/rc

Conflicts of Interest: All authors have completed the ICMJE uniform disclosure form (available at https://jtd.amegroups.com/article/view/10.21037/jtd-22-86/coif). The authors have no conflicts of interest to declare.

Ethical Statement: The authors are accountable for all aspects of the work in ensuring that questions related to the accuracy or integrity of any part of the work are appropriately investigated and resolved. The study was conducted in accordance with the Declaration of Helsinki (as revised in 2013).

References

1. Bade BC, Dela Cruz CS. Lung Cancer 2020: Epidemiology, Etiology, and Prevention. Clin Chest Med 2020;41:1-24.
2. Siegel RL, Miller KD, Jemal A. Cancer statistics, 2019. CA Cancer J Clin 2019;69:7-34.
3. Hirsch FR, Scagliotti GV, Mulshine JL, et al. Lung cancer: current therapies and new targeted treatments. Lancet 2017;389:299-311.
4. Inage T, Nakajima T, Yoshino I, et al. Early Lung Cancer Detection. Clin Chest Med 2018;39:45-55.
5. Kayagaki N, Dixit VM. Rescue from a fiery death: A therapeutic endeavor. Science 2019;366:688-9.
6. Gao J, Qiu X, Xi G, et al. Downregulation of GSDMD attenuates tumor proliferation via the intrinsic mitochondrial apoptotic pathway and inhibition of EGFR/Akt signaling and predicts a good prognosis in non-small cell lung cancer. Oncol Rep 2018;40:1971-84.
7. Galluzzi L, Vitale I, Aaronson SA, et al. Molecular mechanisms of cell death: recommendations of the Nomenclature Committee on Cell Death 2018. Cell Death Differ 2018;25:486-541.
8. Jorgensen I, Rayamajhi M, Miao EA. Programmed cell death as a defence against infection. Nat Rev Immunol 2017;17:151-64.
9. Fang Y, Tian S, Pan Y, et al. Pyroptosis: A new frontier in cancer. Biomed Pharmacother 2020;121:109595.
10. Chen X, He WT, Hu L, et al. Pyroptosis is driven by non-selective gasdermin-D pore and its morphology is different from MLKL channel-mediated necroptosis. Cell Res 2016;26:1007-20.
11. Elmore S. Apoptosis: a review of programmed cell death. Toxicol Pathol 2007;35:495-516.
12. Shi J, Zhao Y, Wang K, et al. Cleavage of GSDMD by inflammatory caspases determines pyroptotic cell death. Nature 2015;526:660-5.
13. Kayagaki N, Stowe IB, Lee BL, et al. Caspase-11 cleaves gasdermin D for non-canonical inflammasome signalling. Nature 2015;526:666-71.
14. Teng JF, Mei QB, Zhou XG, et al. Polyphyllin VI Induces

Caspase-1-Mediated Pyroptosis via the Induction of ROS/NF-κB/NLRP3/GSDMD Signal Axis in Non-Small Cell Lung Cancer. Cancers (Basel) 2020;12:193.
15. Wang Y, Gao W, Shi X, et al. Chemotherapy drugs induce pyroptosis through caspase-3 cleavage of a gasdermin. Nature 2017;547:99-103.
16. Zhang CC, Li CG, Wang YF, et al. Chemotherapeutic paclitaxel and cisplatin differentially induce pyroptosis in A549 lung cancer cells via caspase-3/GSDME activation. Apoptosis 2019;24:312-25.
17. Lin W, Chen Y, Wu B, et al. Identification of the pyroptosis-related prognostic gene signature and the associated regulation axis in lung adenocarcinoma. Cell Death Discov 2021;7:161.
18. Liu LP, Lu L, Zhao QQ, et al. Identification and Validation of the Pyroptosis-Related Molecular Subtypes of Lung Adenocarcinoma by Bioinformatics and Machine Learning. Front Cell Dev Biol 2021;9:756340.
19. Zhang G, Yan Z. A New Definition of Pyroptosis-Related Gene Markers to Predict the Prognosis of Lung Adenocarcinoma. Biomed Res Int 2021;2021:8175003.
20. Li L, Jiang M, Qi L, et al. Pyroptosis, a new bridge to tumor immunity. Cancer Sci 2021;112:3979-94.
21. Herbst RS, Morgensztern D, Boshoff C. The biology and management of non-small cell lung cancer. Nature 2018;553:446-54.
22. Gainor JF, Shaw AT. Emerging paradigms in the development of resistance to tyrosine kinase inhibitors in lung cancer. J Clin Oncol 2013;31:3987-96.
23. Devarakonda S, Morgensztern D, Govindan R. Genomic alterations in lung adenocarcinoma. Lancet Oncol 2015;16:e342-51.
24. Calvayrac O, Pradines A, Pons E, et al. Molecular biomarkers for lung adenocarcinoma. Eur Respir J 2017;49:1601734.
25. Tang R, Xu J, Zhang B, et al. Ferroptosis, necroptosis, and pyroptosis in anticancer immunity. J Hematol Oncol 2020;13:110.
26. Chen L, Weng B, Li H, et al. A thiopyran derivative with low murine toxicity with therapeutic potential on lung cancer acting through a NF-κB mediated apoptosis-to-pyroptosis switch. Apoptosis 2019;24:74-82.
27. Wang WJ, Chen D, Jiang MZ, et al. Downregulation of gasdermin D promotes gastric cancer proliferation by regulating cell cycle-related proteins. J Dig Dis 2018;19:74-83.
28. Li Q, Chen L, Dong Z, et al. Piperlongumine analogue L50377 induces pyroptosis via ROS mediated NF-κB suppression in non-small-cell lung cancer. Chem Biol Interact 2019;313:108820.
29. Tapeinos C, Pandit A. Physical, Chemical, and Biological Structures based on ROS-Sensitive Moieties that are Able to Respond to Oxidative Microenvironments. Adv Mater 2016;28:5553-85.
30. Le X, Mu J, Peng W, et al. DNA methylation downregulated ZDHHC1 suppresses tumor growth by altering cellular metabolism and inducing oxidative/ER stress-mediated apoptosis and pyroptosis. Theranostics 2020;10:9495-511.
31. Wu M, Wang Y, Yang D, et al. A PLK1 kinase inhibitor enhances the chemosensitivity of cisplatin by inducing pyroptosis in oesophageal squamous cell carcinoma. EBioMedicine 2019;41:244-55.
32. Cuylen S, Blaukopf C, Politi AZ, et al. Ki-67 acts as a biological surfactant to disperse mitotic chromosomes. Nature 2016;535:308-12.
33. Menon SS, Guruvayoorappan C, Sakthivel KM, et al. Ki-67 protein as a tumour proliferation marker. Clin Chim Acta 2019;491:39-45.
34. Chirieac LR. Ki-67 expression in pulmonary tumors. Transl Lung Cancer Res 2016;5:547-51.
35. Li Z, Li F, Pan C, et al. Tumor cell proliferation (Ki-67) expression and its prognostic significance in histological subtypes of lung adenocarcinoma. Lung Cancer 2021;154:69-75.
36. Wang F, Liu W, Ning J, et al. Simvastatin Suppresses Proliferation and Migration in Non-small Cell Lung Cancer via Pyroptosis. Int J Biol Sci 2018;14:406-17.
37. Burger JA, Wiestner A. Targeting B cell receptor signalling in cancer: preclinical and clinical advances. Nat Rev Cancer 2018;18:148-67.
38. Yang X, Zheng Y, Han Z, et al. Functions and clinical significance of KLRG1 in the development of lung adenocarcinoma and immunotherapy. BMC Cancer 2021;21:752.
39. Molina-Cerrillo J, Alonso-Gordoa T, Gajate P, et al. Bruton's tyrosine kinase (BTK) as a promising target in solid tumors. Cancer Treat Rev 2017;58:41-50.
40. Hong D, Rasco D, Veeder M, et al. A Phase 1b/2 Study of the Bruton Tyrosine Kinase Inhibitor Ibrutinib and the PD-L1 Inhibitor Durvalumab in Patients with Pretreated Solid Tumors. Oncology 2019;97:102-11.
41. Hu J, Zhang H, Cao M, et al. Auranofin Enhances Ibrutinib's Anticancer Activity in EGFR-Mutant Lung Adenocarcinoma. Mol Cancer Ther 2018;17:2156-63.
42. Gao W, Wang M, Wang L, et al. Selective antitumor activity of ibrutinib in EGFR-mutant non-small cell lung cancer cells. J Natl Cancer Inst 2014;106:dju204.

43. Giordano F, Vaira V, Cortinovis D, et al. p65BTK is a novel potential actionable target in KRAS-mutated/EGFR-wild type lung adenocarcinoma. J Exp Clin Cancer Res 2019;38:260.
44. Bi KW, Wei XG, Qin XX, et al. BTK Has Potential to Be a Prognostic Factor for Lung Adenocarcinoma and an Indicator for Tumor Microenvironment Remodeling: A Study Based on TCGA Data Mining. Front Oncol 2020;10:424.
45. Rada M, Barlev N, Macip S. BTK: a two-faced effector in cancer and tumour suppression. Cell Death Dis 2018;9:1064.
46. Althubiti M, Rada M, Samuel J, et al. BTK Modulates p53 Activity to Enhance Apoptotic and Senescent Responses. Cancer Res 2016;76:5405-14.
47. Janke C, Magiera MM. The tubulin code and its role in controlling microtubule properties and functions. Nat Rev Mol Cell Biol 2020;21:307-26.
48. Lopes D, Maiato H. The Tubulin Code in Mitosis and Cancer. Cells 2020;9:2356.
49. Shao Q, Yang T, Huang H, et al. Uncoupling of UNC5C with Polymerized TUBB3 in Microtubules Mediates Netrin-1 Repulsion. J Neurosci 2017;37:5620-33.
50. Gonçalves A, Braguer D, Kamath K, et al. Resistance to Taxol in lung cancer cells associated with increased microtubule dynamics. Proc Natl Acad Sci U S A 2001;98:11737-42.
51. Haider K, Rahaman S, Yar MS, et al. Tubulin inhibitors as novel anticancer agents: an overview on patents (2013-2018). Expert Opin Ther Pat 2019;29:623-41.
52. Borisy G, Heald R, Howard J, et al. Microtubules: 50 years on from the discovery of tubulin. Nat Rev Mol Cell Biol 2016;17:322-8.
53. Hardin C, Shum E, Singh AP, et al. Emerging treatment using tubulin inhibitors in advanced non-small cell lung cancer. Expert Opin Pharmacother 2017;18:701-16.
54. Kavallaris M. Microtubules and resistance to tubulin-binding agents. Nat Rev Cancer 2010;10:194-204.
55. Sève P, Dumontet C. Is class III beta-tubulin a predictive factor in patients receiving tubulin-binding agents? Lancet Oncol 2008;9:168-75.
56. Cucchiarelli V, Hiser L, Smith H, et al. Beta-tubulin isotype classes II and V expression patterns in nonsmall cell lung carcinomas. Cell Motil Cytoskeleton 2008;65:675-85.
57. Huang L, Fang X, Shi D, et al. MSP-RON Pathway: Potential Regulator of Inflammation and Innate Immunity. Front Immunol 2020;11:569082.
58. Angeloni D, Danilkovitch-Miagkova A, Ivanov SV, et al. Gene structure of the human receptor tyrosine kinase RON and mutation analysis in lung cancer samples. Genes Chromosomes Cancer 2000;29:147-56.
59. Yao HP, Zhou YQ, Zhang R, et al. MSP-RON signalling in cancer: pathogenesis and therapeutic potential. Nat Rev Cancer 2013;13:466-81.
60. Wagh PK, Peace BE, Waltz SE. Met-related receptor tyrosine kinase Ron in tumor growth and metastasis. Adv Cancer Res 2008;100:1-33.
61. Kanteti R, Krishnaswamy S, Catenacci D, et al. Differential expression of RON in small and non-small cell lung cancers. Genes Chromosomes Cancer 2012;51:841-51.
62. Willett CG, Wang MH, Emanuel RL, et al. Macrophage-stimulating protein and its receptor in non-small-cell lung tumors: induction of receptor tyrosine phosphorylation and cell migration. Am J Respir Cell Mol Biol 1998;18:489-96.
63. Van de Laar E, Clifford M, Hasenoeder S, et al. Cell surface marker profiling of human tracheal basal cells reveals distinct subpopulations, identifies MST1/MSP as a mitogenic signal, and identifies new biomarkers for lung squamous cell carcinomas. Respir Res 2014;15:160.
64. Kurebayashi Y, Emoto K, Hayashi Y, et al. Comprehensive Immune Profiling of Lung Adenocarcinomas Reveals Four Immunosubtypes with Plasma Cell Subtype a Negative Indicator. Cancer Immunol Res 2016;4:234-47.
65. Jumaa H, Hendriks RW, Reth M. B cell signaling and tumorigenesis. Annu Rev Immunol 2005;23:415-45.
66. Chen Y, Chen H, Mao B, et al. Transcriptional Characterization Of The Tumor Immune Microenvironment And Its Prognostic Value For Locally Advanced Lung Adenocarcinoma In A Chinese Population. Cancer Manag Res 2019;11:9165-73.
67. Weber ANR, Bittner Z, Liu X, et al. Bruton's Tyrosine Kinase: An Emerging Key Player in Innate Immunity. Front Immunol 2017;8:1454.
68. Noy R, Pollard JW. Tumor-associated macrophages: from mechanisms to therapy. Immunity 2014;41:49-61.
69. Cheng N, Bai X, Shu Y, et al. Targeting tumor-associated macrophages as an antitumor strategy. Biochem Pharmacol 2021;183:114354.
70. Sun L, Jiang G, Gonzalez-Rivas D, et al. An individualized immune prognostic signature in lung adenocarcinoma. Cancer Cell Int 2020;20:156.

(English Language Editor: J. Jones)

Cite this article as: Lin X, Zhou T, Hu S, Yang L, Yang Z, Pang H, Zhou X, Zhong R, Fang X, Yu Z, Hu K. Prognostic significance of pyroptosis-related factors in lung adenocarcinoma. J Thorac Dis 2022;14(3):654-667. doi: 10.21037/jtd-22-86

Table S1 Pyroptosis-related genes derived from the GeneCards database

Gene symbol	Description	Category	Gifts	GC Id	Relevance score	GeneCards Link
GSDMD	Gasdermin D	Protein coding	39	GC08P143553	20.79	https://www.genecards.org/cgi-bin/carddisp.pl?gene=GSDMD
GSDME	Gasdermin E	Protein coding	31	GC07M024699	14.54	https://www.genecards.org/cgi-bin/carddisp.pl?gene=GSDME
NLRP3	NLR family pyrin domain containing 3	Protein coding	47	GC01P247415	12.89	https://www.genecards.org/cgi-bin/carddisp.pl?gene=NLRP3
CASP4	Caspase 4	Protein coding	46	GC11M104942	9.79	https://www.genecards.org/cgi-bin/carddisp.pl?gene=CASP4
GSDMB	Gasdermin B	Protein coding	36	GC17M039904	9.77	https://www.genecards.org/cgi-bin/carddisp.pl?gene=GSDMB
NLRC4	NLR family CARD domain containing 4	Protein coding	44	GC02M032224	8.04	https://www.genecards.org/cgi-bin/carddisp.pl?gene=NLRC4
GSDMA	Gasdermin A	Protein coding	36	GC17P039962	7.49	https://www.genecards.org/cgi-bin/carddisp.pl?gene=GSDMA
GSDMC	Gasdermin C	Protein coding	32	GC08M129705	7.49	https://www.genecards.org/cgi-bin/carddisp.pl?gene=GSDMC
CASP1	Caspase 1	Protein coding	50	GC11M105025	7.26	https://www.genecards.org/cgi-bin/carddisp.pl?gene=CASP1
IL1B	Interleukin 1 beta	Protein coding	48	GC02M112829	7.21	https://www.genecards.org/cgi-bin/carddisp.pl?gene=IL1B
NLRP1	NLR family pyrin domain containing 1	Protein coding	44	GC17M005499	7.02	https://www.genecards.org/cgi-bin/carddisp.pl?gene=NLRP1
NAIP	NLR family apoptosis inhibitory protein	Protein coding	40	GC05M070968	6.17	https://www.genecards.org/cgi-bin/carddisp.pl?gene=NAIP
PYCARD	PYD and CARD domain containing	Protein coding	43	GC16M031201	5.64	https://www.genecards.org/cgi-bin/carddisp.pl?gene=PYCARD
DHX9	DExH-box helicase 9	Protein coding	40	GC01P182839	5.48	https://www.genecards.org/cgi-bin/carddisp.pl?gene=DHX9
NLRP9	NLR family pyrin domain containing 9	Protein coding	34	GC19M055711	5.48	https://www.genecards.org/cgi-bin/carddisp.pl?gene=NLRP9
APIP	APAF1 interacting protein	Protein coding	39	GC11M034854	5.19	https://www.genecards.org/cgi-bin/carddisp.pl?gene=APIP
AIM2	Absent In melanoma 2	Protein coding	41	GC01M159062	4.75	https://www.genecards.org/cgi-bin/carddisp.pl?gene=AIM2
CASP3	Caspase 3	Protein coding	50	GC04M184627	3.93	https://www.genecards.org/cgi-bin/carddisp.pl?gene=CASP3
DDX3X	DEAD-box helicase 3 X-linked	Protein coding	47	GC0XP041333	3.43	https://www.genecards.org/cgi-bin/carddisp.pl?gene=DDX3X
KCNQ1OT1	KCNQ1 opposite strand/antisense transcript 1	Rna gene	25	GC11M002661	3.36	https://www.genecards.org/cgi-bin/carddisp.pl?gene=KCNQ1OT1
FOXO3	Forkhead box O3	Protein coding	44	GC06P108559	3.26	https://www.genecards.org/cgi-bin/carddisp.pl?gene=FOXO3
CPTP	Ceramide-1-phosphate transfer protein	Protein coding	31	GC01P001475	3.09	https://www.genecards.org/cgi-bin/carddisp.pl?gene=CPTP
IL18	Interleukin 18	Protein coding	44	GC11M112143	2.83	https://www.genecards.org/cgi-bin/carddisp.pl?gene=IL18
HMGB1	High mobility group box 1	Protein coding	44	GC13M030456	2.51	https://www.genecards.org/cgi-bin/carddisp.pl?gene=HMGB1
CASP5	Caspase 5	Protein coding	44	GC11M104995	2.45	https://www.genecards.org/cgi-bin/carddisp.pl?gene=CASP5
GJA1	Gap junction protein alpha 1	Protein coding	50	GC06P121436	2.41	https://www.genecards.org/cgi-bin/carddisp.pl?gene=GJA1
MIR30C1	MicroRNA 30c-1	Rna gene	21	GC01P040757	2.37	https://www.genecards.org/cgi-bin/carddisp.pl?gene=MIR30C1
MIR214	MicroRNA 214	Rna gene	20	GC01M172234	2.35	https://www.genecards.org/cgi-bin/carddisp.pl?gene=MIR214
MALAT1	Metastasis associated lung adenocarcinoma transcript 1	Rna gene	24	GC11P065806	2.33	https://www.genecards.org/cgi-bin/carddisp.pl?gene=MALAT1
MIR22	MicroRNA 22	Rna gene	20	GC17M001713	2.33	https://www.genecards.org/cgi-bin/carddisp.pl?gene=MIR22
TP53	Tumor protein P53	Protein coding	54	GC17M007661	2.28	https://www.genecards.org/cgi-bin/carddisp.pl?gene=TP53
TET2	Tet methylcytosine dioxygenase 2	Protein coding	44	GC04P105145	2.24	https://www.genecards.org/cgi-bin/carddisp.pl?gene=TET2
MIR125A	MicroRNA 125a	Rna gene	21	GC19P051720	2.24	https://www.genecards.org/cgi-bin/carddisp.pl?gene=MIR125A
MIR155	MicroRNA 155	Rna gene	18	GC21P025573	2.24	https://www.genecards.org/cgi-bin/carddisp.pl?gene=MIR155
EEF2K	Eukaryotic elongation factor 2 kinase	Protein coding	47	GC16P022217	2.18	https://www.genecards.org/cgi-bin/carddisp.pl?gene=EEF2K
P2RX7	Purinergic receptor P2X 7	Protein coding	45	GC12P122829	2.18	https://www.genecards.org/cgi-bin/carddisp.pl?gene=P2RX7
FGF21	Fibroblast growth factor 21	Protein coding	40	GC19P048766	2.18	https://www.genecards.org/cgi-bin/carddisp.pl?gene=FGF21
MIR135B	MicroRNA 135b	Rna gene	19	GC01M205448	2.13	https://www.genecards.org/cgi-bin/carddisp.pl?gene=MIR135B
MALT1	MALT1 paracaspase	Protein coding	47	GC18P058671	2.11	https://www.genecards.org/cgi-bin/carddisp.pl?gene=MALT1
STK4	Serine/threonine kinase 4	Protein coding	48	GC20P044966	2.06	https://www.genecards.org/cgi-bin/carddisp.pl?gene=STK4
MST1	Macrophage stimulating 1	Protein coding	44	GC03M049683	2.06	https://www.genecards.org/cgi-bin/carddisp.pl?gene=MST1
TREM2	Triggering receptor expressed on myeloid cells 2	Protein coding	43	GC06M042280	2.06	https://www.genecards.org/cgi-bin/carddisp.pl?gene=TREM2
GZMA	Granzyme A	Protein coding	42	GC05P055102	2.06	https://www.genecards.org/cgi-bin/carddisp.pl?gene=GZMA
GBP1	Guanylate binding protein 1	Protein coding	41	GC01M089052	2.06	https://www.genecards.org/cgi-bin/carddisp.pl?gene=GBP1
ELAVL1	ELAV like RNA binding protein 1	Protein coding	41	GC19M007958	2.06	https://www.genecards.org/cgi-bin/carddisp.pl?gene=ELAVL1
MIR9-1	MicroRNA 9-1	Rna gene	20	GC01M156420	2.06	https://www.genecards.org/cgi-bin/carddisp.pl?gene=MIR9-1
MIR9-3	MicroRNA 9-3	Rna gene	19	GC15P089363	2.06	https://www.genecards.org/cgi-bin/carddisp.pl?gene=MIR9-3
MIR9-2	MicroRNA 9-2	Rna gene	18	GC05M088666	2.06	https://www.genecards.org/cgi-bin/carddisp.pl?gene=MIR9-2
HDAC6	Histone deacetylase 6	Protein coding	51	GC0XP048801	1.99	https://www.genecards.org/cgi-bin/carddisp.pl?gene=HDAC6
SQSTM1	Sequestosome 1	Protein coding	48	GC05P179806	1.99	https://www.genecards.org/cgi-bin/carddisp.pl?gene=SQSTM1
IRF3	Interferon regulatory factor 3	Protein coding	47	GC19M049659	1.99	https://www.genecards.org/cgi-bin/carddisp.pl?gene=IRF3
STING1	Stimulator of interferon response CGAMP interactor 1	Protein coding	34	GC05M139476	1.99	https://www.genecards.org/cgi-bin/carddisp.pl?gene=STING1
HNP1	Hypertensive nephropathy	Genetic locus	2	GC09U900671	1.99	https://www.genecards.org/cgi-bin/carddisp.pl?gene=HNP1
CAMP	Cathelicidin antimicrobial peptide	Protein coding	41	GC03P048266	1.66	https://www.genecards.org/cgi-bin/carddisp.pl?gene=CAMP
PARP1	Poly(ADP-ribose) polymerase 1	Protein coding	49	GC01M226360	1.6	https://www.genecards.org/cgi-bin/carddisp.pl?gene=PARP1
GBP5	Guanylate binding protein 5	Protein coding	37	GC01M089259	1.6	https://www.genecards.org/cgi-bin/carddisp.pl?gene=GBP5
NR1H2	Nuclear receptor subfamily 1 group H member 2	Protein coding	48	GC19P050329	1.53	https://www.genecards.org/cgi-bin/carddisp.pl?gene=NR1H2
CTSG	Cathepsin G	Protein coding	44	GC14M024573	1.46	https://www.genecards.org/cgi-bin/carddisp.pl?gene=CTSG
MKI67	Marker of proliferation Ki-67	Protein coding	44	GC10M128096	1.46	https://www.genecards.org/cgi-bin/carddisp.pl?gene=MKI67
IL36G	Interleukin 36 gamma	Protein coding	38	GC02P112973	1.36	https://www.genecards.org/cgi-bin/carddisp.pl?gene=IL36G
IL36B	Interleukin 36 beta	Protein coding	35	GC02M113022	1.36	https://www.genecards.org/cgi-bin/carddisp.pl?gene=IL36B
ANO6	Anoctamin 6	Protein coding	39	GC12P045215	1.07	https://www.genecards.org/cgi-bin/carddisp.pl?gene=ANO6
FADD	Fas associated via death domain	Protein coding	47	GC11P070203	1.01	https://www.genecards.org/cgi-bin/carddisp.pl?gene=FADD
NLRP7	NLR family pyrin domain containing 7	Protein coding	43	GC19M054923	1.01	https://www.genecards.org/cgi-bin/carddisp.pl?gene=NLRP7
TNF	Tumor necrosis factor	Protein coding	51	GC06P047305	0.94	https://www.genecards.org/cgi-bin/carddisp.pl?gene=TNF
VIM	Vimentin	Protein coding	50	GC10P017227	0.94	https://www.genecards.org/cgi-bin/carddisp.pl?gene=VIM
CAPN1	Calpain 1	Protein coding	49	GC11P065198	0.94	https://www.genecards.org/cgi-bin/carddisp.pl?gene=CAPN1
PRTN3	Proteinase 3	Protein coding	44	GC19P000840	0.87	https://www.genecards.org/cgi-bin/carddisp.pl?gene=PRTN3
MEFV	MEFV innate immunity regulator, pyrin	Protein coding	43	GC16M003281	0.87	https://www.genecards.org/cgi-bin/carddisp.pl?gene=MEFV
SERPINB1	Serpin family B member 1	Protein coding	40	GC06M002833	0.87	https://www.genecards.org/cgi-bin/carddisp.pl?gene=SERPINB1
ALK	ALK receptor tyrosine kinase	Protein coding	51	GC02M029156	0.77	https://www.genecards.org/cgi-bin/carddisp.pl?gene=ALK
SIRT1	Sirtuin 1	Protein coding	49	GC10P067884	0.77	https://www.genecards.org/cgi-bin/carddisp.pl?gene=SIRT1
BIRC3	Baculoviral IAP repeat containing 3	Protein coding	46	GC11P102317	0.77	https://www.genecards.org/cgi-bin/carddisp.pl?gene=BIRC3
BIRC2	Baculoviral IAP repeat containing 2	Protein coding	45	GC11P102347	0.77	https://www.genecards.org/cgi-bin/carddisp.pl?gene=BIRC2
UBE2D2	Ubiquitin conjugating enzyme E2 D2	Protein coding	44	GC05P139526	0.77	https://www.genecards.org/cgi-bin/carddisp.pl?gene=UBE2D2
APOL1	Apolipoprotein L1	Protein coding	42	GC22P036253	0.77	https://www.genecards.org/cgi-bin/carddisp.pl?gene=APOL1
LY96	Lymphocyte antigen 96	Protein coding	42	GC08P073991	0.77	https://www.genecards.org/cgi-bin/carddisp.pl?gene=LY96
GLMN	Glomulin, FKBP associated protein	Protein coding	40	GC01M092246	0.77	https://www.genecards.org/cgi-bin/carddisp.pl?gene=GLMN
IRGM	Immunity related GTPase M	Protein coding	38	GC05P150846	0.77	https://www.genecards.org/cgi-bin/carddisp.pl?gene=IRGM
NLRP13	NLR family pyrin domain containing 13	Protein coding	35	GC19M055892	0.77	https://www.genecards.org/cgi-bin/carddisp.pl?gene=NLRP13
TUBB6	Tubulin beta 6 class V	Protein coding	41	GC18P012307	0.68	https://www.genecards.org/cgi-bin/carddisp.pl?gene=TUBB6
PYDC2	Pyrin domain containing 2	Protein coding	24	GC03P191461	0.53	https://www.genecards.org/cgi-bin/carddisp.pl?gene=PYDC2
AKT1	AKT serine/threonine kinase 1	Protein coding	54	GC14M104769	0.34	https://www.genecards.org/cgi-bin/carddisp.pl?gene=AKT1
EGFR	Epidermal growth factor receptor	Protein coding	54	GC07P055019	0.34	https://www.genecards.org/cgi-bin/carddisp.pl?gene=EGFR
TP63	Tumor protein P63	Protein coding	48	GC03P189598	0.34	https://www.genecards.org/cgi-bin/carddisp.pl?gene=TP63
ATF6	Activating transcription factor 6	Protein coding	47	GC01P161766	0.34	https://www.genecards.org/cgi-bin/carddisp.pl?gene=ATF6
IFI16	Interferon gamma inducible protein 16	Protein coding	42	GC01P158969	0.34	https://www.genecards.org/cgi-bin/carddisp.pl?gene=IFI16
POP1	POP1 homolog, ribonuclease P/MRP subunit	Protein coding	40	GC08P098117	0.34	https://www.genecards.org/cgi-bin/carddisp.pl?gene=POP1
ORMDL3	ORMDL sphingolipid biosynthesis regulator 3	Protein coding	39	GC17M039921	0.34	https://www.genecards.org/cgi-bin/carddisp.pl?gene=ORMDL3
BTK	Bruton tyrosine kinase	Protein coding	53	GC0XM101349	0.24	https://www.genecards.org/cgi-bin/carddisp.pl?gene=BTK
STAT3	Signal transducer and activator of transcription 3	Protein coding	52	GC17M042313	0.24	https://www.genecards.org/cgi-bin/carddisp.pl?gene=STAT3
NFKB1	Nuclear factor kappa B subunit 1	Protein coding	52	GC04P102501	0.24	https://www.genecards.org/cgi-bin/carddisp.pl?gene=NFKB1
BCL2	BCL2 apoptosis regulator	Protein coding	51	GC18M063123	0.24	https://www.genecards.org/cgi-bin/carddisp.pl?gene=BCL2
TLR2	Toll like receptor 2	Protein coding	51	GC04P153684	0.24	https://www.genecards.org/cgi-bin/carddisp.pl?gene=TLR2
ANXA2	Annexin A2	Protein coding	48	GC15M060347	0.24	https://www.genecards.org/cgi-bin/carddisp.pl?gene=ANXA2
BECN1	Beclin 1	Protein coding	46	GC17M042810	0.24	https://www.genecards.org/cgi-bin/carddisp.pl?gene=BECN1
CD14	CD14 molecule	Protein coding	44	GC05M140631	0.24	https://www.genecards.org/cgi-bin/carddisp.pl?gene=CD14
IL13	Interleukin 13	Protein coding	44	GC05P132656	0.24	https://www.genecards.org/cgi-bin/carddisp.pl?gene=IL13
CHI3L1	Chitinase 3 like 1	Protein coding	43	GC01M203148	0.24	https://www.genecards.org/cgi-bin/carddisp.pl?gene=CHI3L1
PANX1	Pannexin 1	Protein coding	43	GC11P094128	0.24	https://www.genecards.org/cgi-bin/carddisp.pl?gene=PANX1
LRPPRC	Leucine rich pentatricopeptide repeat containing	Protein coding	42	GC02M043850	0.24	https://www.genecards.org/cgi-bin/carddisp.pl?gene=LRPPRC
CXCL8	C-X-C motif chemokine ligand 8	Protein coding	41	GC04P073740	0.24	https://www.genecards.org/cgi-bin/carddisp.pl?gene=CXCL8
IL13RA2	Interleukin 13 receptor subunit alpha 2	Protein coding	41	GC0XM115003	0.24	https://www.genecards.org/cgi-bin/carddisp.pl?gene=IL13RA2
IL32	Interleukin 32	Protein coding	40	GC16P004242	0.24	https://www.genecards.org/cgi-bin/carddisp.pl?gene=IL32
BST2	Bone marrow stromal cell antigen 2	Protein coding	39	GC19M017403	0.24	https://www.genecards.org/cgi-bin/carddisp.pl?gene=BST2
LYST	Lysosomal trafficking regulator	Protein coding	38	GC01M235661	0.24	https://www.genecards.org/cgi-bin/carddisp.pl?gene=LYST
GPER1	G protein-coupled estrogen receptor 1	Protein coding	37	GC07P001188	0.24	https://www.genecards.org/cgi-bin/carddisp.pl?gene=GPER1
CLEC5A	C-type lectin domain containing 5A	Protein coding	34	GC07M141927	0.24	https://www.genecards.org/cgi-bin/carddisp.pl?gene=CLEC5A
MIR223	MicroRNA 223	RNA gene	21	GC0XP066018	0.24	https://www.genecards.org/cgi-bin/carddisp.pl?gene=MIR223
MIR20B	MicroRNA 20b	RNA gene	15	GC0XM134217	0.24	https://www.genecards.org/cgi-bin/carddisp.pl?gene=MIR20B

https://dx.doi.org/10.21037/jtd-22-86

Table S2 Results of 26 pyroptosis-related genes identified in differentially expressed analysis in the TCGA-LUAD dataset

Genes	Base mean	LogFC	LfcSE	Stat.	P value	FDR
MKI67	3533.056	−3.32718	0.166517	−19.981	8.06E−89	7.90E−87
NLRC4	254.7377	2.017568	0.104854	19.24172	1.66E−82	8.11E−81
PARP1	9166.919	−1.1725	0.08541	−13.7278	6.92E−43	2.26E−41
IL36G	28.50111	−4.0338	0.31024	−13.0022	1.19E−38	2.91E−37
AIM2	432.8062	−2.83864	0.222915	−12.7342	3.82E−37	7.49E−36
GSDMB	1282.436	−1.89962	0.152084	−12.4906	8.40E−36	1.37E−34
GSDMC	362.4923	−2.73436	0.226562	−12.0689	1.54E−33	2.16E−32
BTK	723.5322	1.323927	0.113146	11.70105	1.26E−31	1.54E−30
MEFV	79.08195	1.588184	0.142912	11.11304	1.08E−28	8.85E−28
POP1	433.3758	−1.04772	0.094749	−11.0579	2.01E−28	1.51E−27
CAMP	39.16229	2.497897	0.237022	10.53866	5.73E−26	3.74E−25
GPER1	216.5156	1.967691	0.190281	10.34097	4.60E−25	2.82E−24
VIM	38237.57	1.050962	0.10463	10.04461	9.70E−24	5.59E−23
TUBB6	2654.095	1.161233	0.12122	9.579564	9.75E−22	5.31E−21
MST1	315.0309	−1.59668	0.172427	−9.26003	2.04E−20	1.00E−19
CASP5	26.71728	1.267633	0.151058	8.39168	4.79E−17	2.13E−16
IL13	4.925103	1.496938	0.187722	7.974239	1.53E−15	6.26E−15
CTSG	80.79507	1.722087	0.231224	7.447685	9.50E−14	3.21E−13
KCNQ1OT1	417.8221	−1.23114	0.172603	−7.13275	9.84E−13	3.11E−12
NLRP7	17.22144	−1.27272	0.187501	−6.78777	1.14E−11	3.28E−11
GJA1	5957.535	1.058294	0.161846	6.5389	6.20E−11	1.74E−10
CHI3L1	8116.59	−1.41656	0.225666	−6.27724	3.45E−10	9.13E−10
GSDMA	67.40323	−1.17423	0.192915	−6.08679	1.15E−09	2.82E−09
MIR135B	2.299623	−1.24253	0.233194	−5.32833	9.91E−08	2.26E−07
FGF21	2.252621	−1.65782	0.37071	−4.47201	7.75E−06	1.62E−05
NLRP13	2.261375	−1.4579	0.390676	−3.73173	0.00019	0.000333

TCGA-LUAD, The Cancer Genome Atlas-lung adenocarcinoma; FC, fold change; lfcSE, standard error for log2 fold change; FDR, false discovery rate.

https://dx.doi.org/10.21037/jtd-22-86

Table S3 Results of 4 key genes in multivariate Cox regression analysis in the TCGA-LUAD dataset

Genes	Coefficient	HR	z	P value
MKI67	0.13	1.1 (1.0–1.3)	2.3	0.024
BTK	–0.27	0.77 (0.67–0.88)	–3.9	1.00E–04
TUBB6	0.23	1.3 (1.1–1.5)	3	0.0032
MST1	–0.14	0.87 (0.76–1.00)	–1.9	0.055

TCGA-LUAD, The Cancer Genome Atlas-lung adenocarcinoma; HR, hazard ratio.

Table S4 Results of clinical variables and 4-gene signature riskScore in univariate Cox regression analysis in the TCGA-LUAD dataset

Variables	Coefficient	HR (95% CI for HR)	Wald test	z	P value
Gender	0.057	1.1 (0.76–1.5)	0.11	0.33	0.74
pathologic_N_stage	–0.92	0.4 (0.28–0.56)	28	–5.3	1.20E–07
pathologic_M_stage	0.61	1.8 (1–3.3)	4.4	2.1	0.037
pathologic_T_stage	0.46	1.6 (1.3-1.9)	21	4.5	5.90E–06
tumor_stage	0.46	1.6 (1.3–1.8)	32	5.7	1.30E–08
Age	–0.34	0.71 (0.4–1.3)	1.4	–1.2	0.24
riskScore	0.67	2 (1.6–2.4)	49	7	2.30E–12

TCGA-LUAD, The Cancer Genome Atlas-lung adenocarcinoma; HR, hazard ratio; CI, confidence interval.

Table S5 Results of clinical variables and 4-gene signature riskScore in multivariate Cox regression analysis in the TCGA-LUAD dataset

Variables	Coefficient	HR	z	P value
pathologic_N_stage	–0.56	0.57 (0.34–0.97)	–2.1	0.036
pathologic_M_stage	0.065	1.1 (0.42–2.7)	0.14	0.89
pathologic_T_stage	0.25	1.3 (1.0–1.6)	2.2	0.03
tumor_stage	0.15	1.2 (0.81–1.7)	0.82	0.41
riskScore	0.6	1.8 (1.5–2.2)	5.8	5.20E–09

TCGA-LUAD, The Cancer Genome Atlas-lung adenocarcinoma; HR, hazard ratio.

https://dx.doi.org/10.21037/jtd-22-86